



## A theoretical and experimental investigation of Eu-doped ZnO nanorods and its application on dye sensitized solar cells

André Felipe Vale da Fonseca <sup>a</sup>, Renato Luiz Siqueira <sup>b</sup>, Richard Landers <sup>c</sup>, Jefferson Luis Ferrari <sup>a</sup>, Naiara L. Marana <sup>d</sup>, Júlio R. Sambrano <sup>d</sup>, Felipe de Almeida La Porta <sup>e</sup>, Marco Antônio Schiavon <sup>a,\*</sup>

<sup>a</sup> Grupo de Pesquisa em Química de Materiais (GPQM), Departamento de Ciências Naturais (DCNat), Universidade Federal de São João del Rei (UFSJ) - Campus Dom Bosco, Praça Dom Helvécio, 74, São João Del Rei, Minas Gerais, 36301-160, Brazil

<sup>b</sup> Laboratório de Materiais Vítreos (LaMaV), Departamento de Engenharia de Materiais, Universidade Federal de São Carlos (UFSCar) - São Carlos, São Paulo, 13565-905, Brazil

<sup>c</sup> Instituto de Física 'Gleb Wataghin' (IFGW), Departamento de Física Aplicada, Universidade Estadual de Campinas (UNICAMP) – Campinas, São Paulo, 13083-859, Brazil

<sup>d</sup> Grupo de Modelagem e Simulação Molecular, Universidade Estadual Paulista (UNESP), Bauru, São Paulo, 17033-360, Brazil

<sup>e</sup> Nanotecnologia e Química Computacional (NanoQC), Departamento de Química, Universidade Tecnológica Federal do Paraná (UTFPR), Londrina, Paraná, 86036-370, Brazil



### ARTICLE INFO

#### Article history:

Received 13 September 2017

Received in revised form

22 December 2017

Accepted 23 December 2017

Available online 28 December 2017

#### Keywords:

Eu-doped ZnO

Nanorods

DSSC

Electrodeposition

DFT calculations

### ABSTRACT

This paper describes the electrodeposition of Europium-doped Zinc Oxide (ZnO) nanorods as well its application as photoanodes in dye sensitized solar cells (DSSCs). The incorporation of the Europium in the ZnO structure was evidenced by X-ray diffraction (XRD) and X-ray photoelectron spectroscopy (XPS). The DSSCs based on Eu-doped nanorods photoanodes exhibits a higher conversion efficiency value ( $\eta$ ) (0.50%) compared to the undoped photoanodes (0.34%). Mott-Schottky analysis was performed and this increase is assigned to the better electronic injection efficiency from the dye to the conduction band of Eu-doped ZnO nanorods, since the Europium incorporation in the ZnO matrix was able to down-shift its conduction band. The improvement on the DSSC performance was around 45%, showing the great potential from the practical point of view. To complement the experimental data, computational simulations were employed based on DFT framework, in order to carry out a detailed analysis of the electronic structures of these materials, as well as to provide an elucidation of its underlying physical mechanism at an atomic level.

© 2017 Elsevier B.V. All rights reserved.

## 1. Introduction

Dye-sensitized solar cells (DSSC), in comparison with the conventional silicon solar cells, are well known as a cost-effective photovoltaic device since they provide comparable power conversion efficiency (PCE) at low manufacturing costs [1,2]. The basic components of DSSC include a semiconductor oxide layer deposited onto a transparent conducting oxide (TCO), dye as sensitizer, a liquid redox electrolyte (usually  $I^-/I^{3-}$  non-aqueous solution), and a counter electrode (usually Pt-coated glass or graphite) [3,4]. This

device was first reported by O'Regan and Grätzel in 1991, where the performance of nanostructured  $TiO_2$  porous films as photoanodes was shown [5].

Many recent studies consider the Zinc oxide (ZnO) as the most promising alternative to the  $TiO_2$  to improve the photovoltaic performance of the dye-sensitized solar cells [6–8]. ZnO is one of the most relevant II-VI binary compound semiconductors, with a wide direct band gap (~3.37 eV) and large exciton binding energy (60 meV) at room temperature [9,10]. The ZnO has advantages over the porous  $TiO_2$ , such as higher electron diffusivity, a higher electron mobility, is available at low-cost, and stability against photo-corrosion [11,12]. In addition, the polar surfaces of the wurtzite crystalline structure enables the growth of many kinds of ZnO nanostructures [13], including nanowires [14], nanorods [15], nanobelts [16], nanosprings [17], nanorings [18], nanobowls [19],

\* Corresponding author. Universidade Federal de São João del Rei, Departamento de Ciências Naturais, Campus Dom Bosco, Praça Dom Helvécio, 74 - Fábricas, São João Del Rei, MG, Brazil.

E-mail address: [schiavon@ufsj.edu.br](mailto:schiavon@ufsj.edu.br) (M.A. Schiavon).

nanoflowers [20], and nanohelices [21]. Among all these structures, in particular, the one dimensional (1-D) ZnO nanostructures, like as nanorods and nanowires, have received increasing attention in recent years, due to its excellent physical and chemical properties, which can provide an effective direct pathway for rapid transport of the photoelectrons and a higher surface area for dye adsorption, enhancing the photovoltaic performance of the DSSCs [22–24]. However, the efficiencies presented by the ZnO based devices are still far behind those of TiO<sub>2</sub> (less than 8%) [25] and a few studies have been highlighted in this field with the aim of improving the PCE of DSSCs based on ZnO nanostructures [9].

In order to improve the electron transport mechanism in the ZnO photoanode or to suppress the recombination reactions between the conduction band (CB) of ZnO and the redox electrolyte, several elements were inserted into the structure of ZnO [11,26]. In order to improve the electrical and optical properties, usually group II, III, IV, V, and VI elements have been chosen to dope into the ZnO host matrix [27]. Particularly, electrical resistivity of ZnO nanorods can be greatly reduced by trivalent cation replacement, such as aluminum, indium, gallium, and boron [28,29].

Huang et al. presented better charge transfer and collection of the Al-doped ZnO nanorods, resulting in solar cells with PCE at about 23% higher than the cells based on non-doped ZnO nanorods [30]. Swapna et al. studied the electrical properties of Eu-doped ZnO thin films prepared by spray pyrolysis and demonstrated that the electrical resistivity of ZnO films was greatly decreased with the Europium incorporation [31]. Recently, hierarchically structured Eu-doped ZnO nanocrystalline aggregates were synthesized through a solvothermal method. Additionally, the DSSCs fabricated using the Eu-doped ZnO aggregates as photoanode exhibits effective electron injection and enhanced electron transport properties, which greatly improve the PCE compared with undoped ZnO aggregates based on DSSCs [32].

In this work, Eu-doped ZnO nanorods were synthesized by electrochemical-hydrothermal method and then applied as the photoanode in DSSCs. X-ray diffraction (XRD), field-emission scanning electron microscopy (FESEM), X-ray photoelectron spectroscopy (XPS), ultraviolet-visible (UV-vis) diffuse-reflectance spectroscopy and electrochemical measurements have been employed to characterize these materials as well as to evaluate their performance in DSSCs applications. To complement experimental data, computational simulations were employed based on DFT framework, in order to carry out a detailed analysis of the electronic structures of these materials, as well as, to provide an elucidation of its underlying physical mechanism at an atomic level.

## 2. Experimental

### 2.1. Chemicals

Zinc Nitrate hexahydrate [Zn(NO<sub>3</sub>)<sub>2</sub>·6H<sub>2</sub>O] (99.0%), Hexamethylenetetramine [C<sub>6</sub>H<sub>12</sub>N<sub>4</sub>] (99.0%), Europium (III) Oxide (99.0%), Sodium Sulfate (98%), Sodium acetate anhydrous (99%), tert-Butanol (99%), Chloroplatinic Acid [H<sub>2</sub>PtCl<sub>6</sub>] (8%), Xylenol Orange and fluorine-doped tin oxide (FTO)-glass Tec-7, were obtained from Sigma-Aldrich; NH<sub>4</sub>OH (P.A.), isopropanol (P.A.), acetic acid (99.7%) and acetone (P.A.) were purchased from Synth; EDTA was obtained from Dynamics; and anhydrous ethanol (99%), HNO<sub>3</sub> (65%), acetonitrile (99.8%) was provided by Vetec. All chemicals were used without further purification.

### 2.2. Eu<sup>3+</sup> solution preparation

The Eu<sup>3+</sup> precursor solution was prepared by reaction between Eu<sub>2</sub>O<sub>3</sub> and HNO<sub>3</sub> 0.1 mol L<sup>-1</sup> under stirring and controlled

temperature (~60 °C). After this step, the solvent was evaporated several times until half volume and completed with water for the acid excess elimination and finally the pH was adjusted to 5.6 with NH<sub>4</sub>OH 0.01 mol L<sup>-1</sup>. The analytical concentration of Eu<sup>3+</sup> ions was determined by complexometric titration with EDTA (0.01 mol L<sup>-1</sup>). The samples were added in an acetic acid/sodium acetate buffer (pH ~5.6) and after the addition of the indicator Xylenol orange the samples were analyzed in triplicates.

### 2.3. Syntheses of ZnO nanorods

The FTO coated glass substrates were subjected to a standard cleaning process using diluted detergent, deionized water, ethanol, isopropanol and acetone for 15 min each, in an ultrasonic bath. In the last step, the substrates were kept in a plasma cleaner for 5 min. The nanorods were deposited by an electrochemical-hydrothermal method using platin wire as counter electrode, Ag/AgCl (KCl 3 mol L<sup>-1</sup>) as reference and pre-cleaned FTO as work electrode. The electrolyte used was an aqueous solution composed by Zinc Nitrate hexahydrate (Zn(NO<sub>3</sub>)<sub>2</sub>·6H<sub>2</sub>O) 0.01 mol L<sup>-1</sup>, Hexamethylenetetramine (HMTA) 0.01 mol L<sup>-1</sup>. For the Eu-doped nanorods, the electrolyte was also composed by Eu<sup>3+</sup> solution 2.5 mmol L<sup>-1</sup> (obtained as 2.2). The deposition was conducted at 90 °C and constant potential -1.0 V during 30 min. After this step the ZnO nanorods arrays were washed with ultrapure water and calcinated at 350 °C for 30 min.

### 2.4. DSSC fabrication

To prepare the DSSCs, Eu-doped ZnO nanorods were immersed in 0.5 mmol L<sup>-1</sup> *cis*-diisothiocyanatobis(2,20-bipyridyl-4,40-dicarboxylato)-ruthenium(II) bis (tetrabutylammonium) (N719, Solaronix). The solvent used to prepare the dye solution consisted of 1:1 mixture of acetonitrile and tert-butanol. Dye sensitization was performed for 2 h at room temperature. After that, the electrodes loaded with N719 were washed with acetonitrile and dried in air. The counter electrode consists of a platinum (Pt) coated FTO glass, which was prepared by placing a drop of H<sub>2</sub>PtCl<sub>6</sub> solution on an FTO glass and subsequently sintering the glass at 400 °C for 1 h. The ZnO photoanode and the platinum counter electrode were sealed together with a hot-melting spacer Parafilm®, and the inner space was filled with a I<sub>3</sub>/I<sup>-</sup> redox electrolyte (Dyesol EL-HPE).

### 2.5. Characterization

The morphology of as-prepared ZnO nanorods were analyzed using a FESEM microscope Phillips FEG X-L30 operating at 10.0 kV. XRD analysis were taken on a Shimadzu XRD 6000 diffractometer with Cu K $\alpha$  radiation ( $\lambda = 1.5418 \text{ \AA}$ ). The UV-Vis reflectance spectra were acquired on an Agilent Cary 5000 UV-Vis-NIR spectrophotometer with a diffuse reflectance analysis module. The XPS spectra were obtained with a VSW HA-100 spherical analyzer with unmonochromatic Al K $\alpha$  radiation ( $h\nu = 1486.6 \text{ eV}$ ). The electrochemical characterizations (photo response, J-V curves and Mott Schottky analysis) were recorded by an electrochemical workstation (Metrohm Autolab PGSTAT302N) with the lighting of a 150 W Xe-Hg lamp (Oriel) equipped with an AM 1.5 G filter and the radiation power was adjusted to 100 mW/cm<sup>2</sup>.

### 2.6. Theoretical models and methods

All computational simulations were carried out by means of a periodic DFT framework with hybrid functional B3LYP, using the CRYSTAL14 package [33]. The atomic centers are described by all electron basis set 86-411d31G39 for Zn atoms [34] and 8-411d140

for O atoms [35], respectively. On the other hand, the Eu atoms is a typical system containing f-orbitals. In general, it is well-known that the f-orbitals of Eu atoms are shielded and consequently they do not contribute significantly for the formation of bonds in several of their compounds [36–38]. Hence, as a computational strategy, in particular, these atoms can easily be described by means of the effective core pseudopotential (ECP) basis set, for this reason the Eu atoms are described in this study by the ECP53MWB-VTZ basis set [39,40]. This methodology has been successfully employed in our previous work [36,41–43].

As a first procedure, the bulk optimizations of the wurtzite ZnO materials structure (belongs to the space group  $P63mc$ ) has been carried out in order to determine the equilibrium geometry, as general result the theoretical parameters obtained was  $a = 3.274 \text{ \AA}$ ,  $c = 5.250 \text{ \AA}$  and  $\nu = 0.383$ , in good agreement with the experimental values. As a second step, the  $2 \times 4 \times 4$  supercell model with 128 atoms ( $\text{Zn}_{64}\text{O}_{64}$ ) was built to study the doping effects in ZnO structure. This model represents doping processes by replacing one Zn atom with one Eu atom, which corresponds to about 6.25 at% Eu concentration in ZnO host matrix (see Fig. 1). For these models, the band structure and density of states (DOS) were analyzed employing 100 k-point sampling as the diagonalization of the Fock-matrix for the optimization process points along appropriate high-symmetry paths of the suitable Brillouin zone.

### 3. Results and discussion

The experiments were performed in aqueous solutions of  $\text{Zn}(\text{NO}_3)_2 \cdot 6\text{H}_2\text{O}$ , HMTA and  $\text{Eu}^{3+}$ , at a potential of  $-1.0 \text{ V}$  and controlled temperature of  $90^\circ\text{C}$ . The electrodeposition mechanism of ZnO is shown as following [44]:

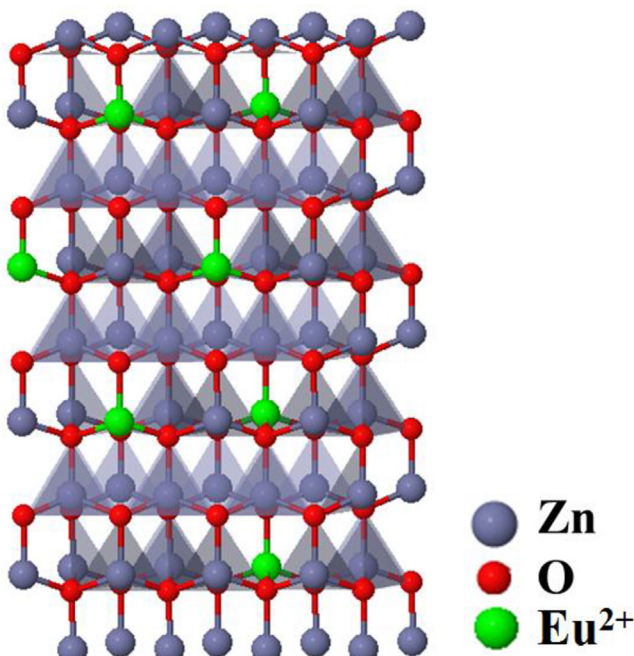
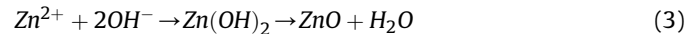
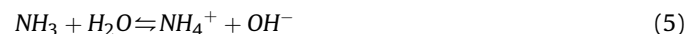


Fig. 1.  $2 \times 4 \times 4$  supercell of Eu-doped ZnO.



The HMTA is one of the most popular organic additives to support the growth of ZnO nanorods of required morphology. In acidic aqueous solution at elevated temperature HMTA hydrolyses as following [45]:



Thus, HMTA acts as an additional source of OH, accelerating the nucleation and growth of nanorods. In addition, the HMTA acts as a buffer, due to the fact that its hydrolysis rate decreases with increasing pH and vice versa [46].

With the presence of  $\text{Eu}^{3+}$  ions, a portion of the  $\text{Eu}^{3+}$  ions can be incorporated as a dopant in the ZnO crystalline lattice and another part of the ions can react with the  $\text{OH}^-$  to form  $\text{Eu}_2\text{O}_3$ . The  $\text{Eu}^{3+}$  reduction may also occur as shown below [47]:



In addition to the basic reactional medium facilitate this process, the potential used in the synthesis of nanorods ( $-1.0 \text{ V}$ ) is more than enough to promote this electrochemical reaction. After that the  $\text{Eu}^{2+}$  can be incorporated into the ZnO lattice as well.

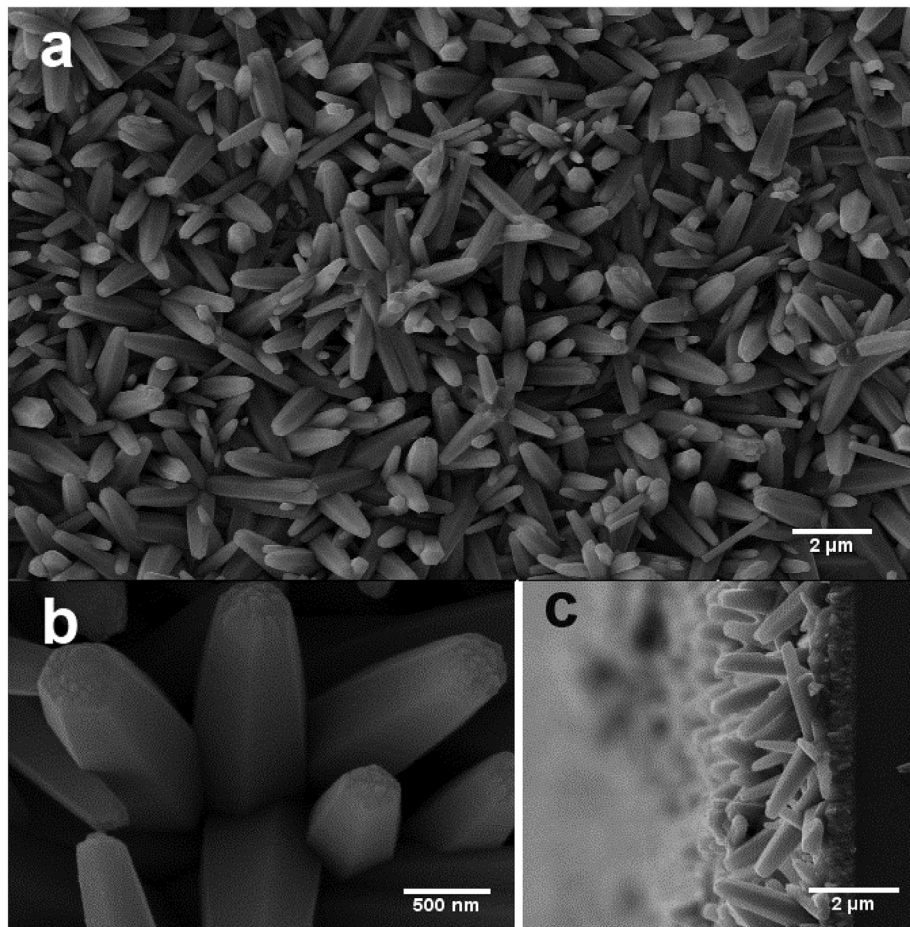
FESEM images were used to investigate the morphology of the Eu-doped ZnO nanorods grown by electrodeposition. An analysis of the results presented in Fig. 2 shows a well-defined morphology of these nanorods, having an average length of approximately  $\sim 2100 \text{ nm}$  with an average diameter of approximately  $\sim 500 \text{ nm}$ , respectively, resulting in an aspect ratio around  $\sim 4.2$ , in good agreement with the other studies [48,49]. In addition, the Eu-doped ZnO nanorods are not perfectly aligned but have a predisposition to grow normally to the surface of the FTO glass (c-axis).

Fig. 3(a) shows the XRD pattern of Eu-doped and undoped ZnO nanorods. In both cases only the hexagonal wurtzite structure of ZnO (JCPDS 36-1451) was evident. All asterisk-marked peaks are assigned to  $\text{SnO}_2:\text{F}$  (FTO) glass structure (JCPDS 01-041-1445) and no additional diffraction peaks, such the  $\text{Eu}_2\text{O}_3$  formation or other impurities were detected. For the undoped ZnO nanorods the peak indexed to (002) crystal direction was the dominant. However, the Eu-doped ZnO nanorods shown considerable intensities for the diffraction peaks referenced to (100) and (101) orientations. This is in accordance with the inclined rods showed in the SEM images (Fig. 2). Fig. 3(b) shows the magnification of (100) diffraction peak evidencing a small shift on  $2\theta$  values for the Eu-doped nanorods. This can be an indication of the  $\text{Zn}^{2+}$  replacement by the  $\text{Eu}^{2+}$  in the lattice, related to fact of the  $\text{Eu}^{2+}$  ionic radii ( $1.17 \text{ \AA}$ ) is larger than that for  $\text{Zn}^{2+}$  ( $0.74 \text{ \AA}$ ), which causes an expansion of the ZnO unit cell volume [32,50].

The microstrain and crystallite size of Eu-doped and pure ZnO nanorods were calculated by the Williamson-Hall (W-H) equation (eq (7)) [51]:

$$\frac{\beta \cos(\theta)}{\lambda} = \frac{0.9}{T} + \frac{\epsilon \sin(\theta)}{\lambda} \quad (7)$$

where  $\beta$  is the width of the peak at half the maximum intensity,  $\theta$  the Bragg diffraction angle,  $\lambda$  the  $\text{K}_\alpha$  radiation ( $\sim 0.15409 \text{ nm}$ ),  $T$  the crystallite size and  $\epsilon$  the microstrain. This model is known as uniform deformation model. Basically, the crystal is assumed to present isotropic nature and lattice strain is considered to be independent of the crystallographic directions [52,53]. Therefore, the strain ( $\epsilon$ ) is estimated from the slope of the W-H line plot and



**Fig. 2.** FESEM images of the ZnO nanorods electrodeposited on FTO substrate: (a) top-view, (b) magnified top-view and (c) lateral-view.

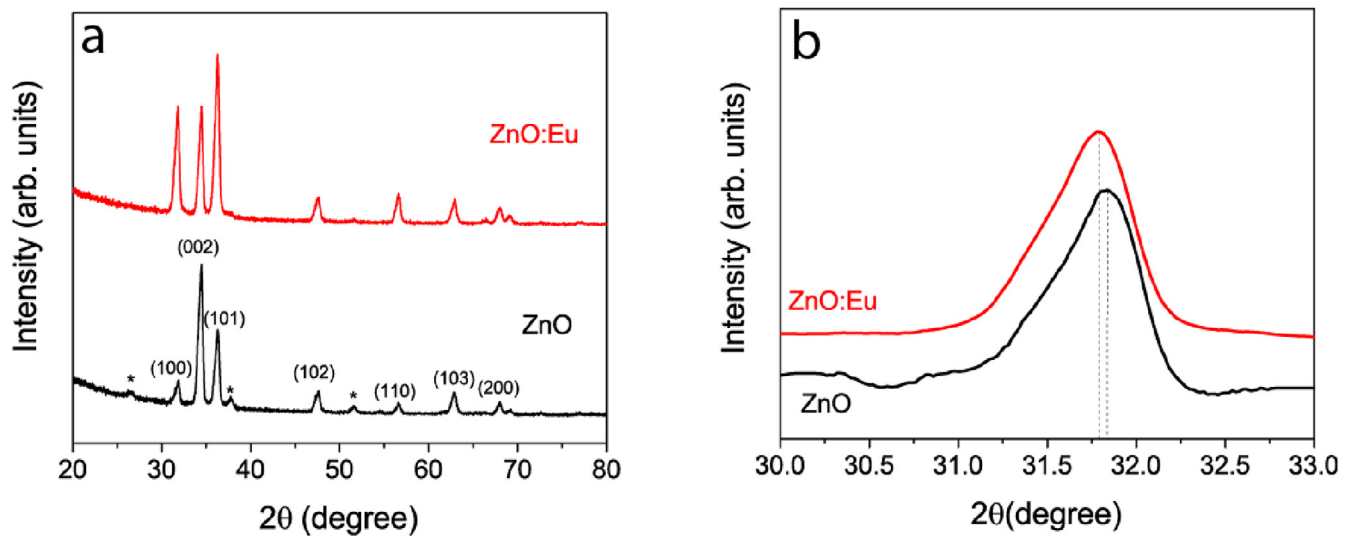


**Fig. 3.** (a) X-ray diffraction pattern of Eu-doped and undoped ZnO nanorods array and (b) the magnification of the shift on peak (100).

the crystallite size ( $T$ ) from the intersection with the vertical axis. Fig. 4 shows the W-H plots of both the samples of ZnO nanorods (Eu-doped and pure ZnO). The crystallite size of undoped and Eu-doped ZnO samples has presented very similar values, estimated as 14 and 17 nm respectively. However, the Eu-doped nanorods

shown higher values of microstrain than undoped ZnO nanorods. This increase in strain value confirms the expansion of the ZnO unit cell volume after the Eu incorporation.

The optical band gap of these nanorods was evaluated by the application of Kubelka-Munk (K-M) equation  $F(R) = (1-R)^2/2R$ ,

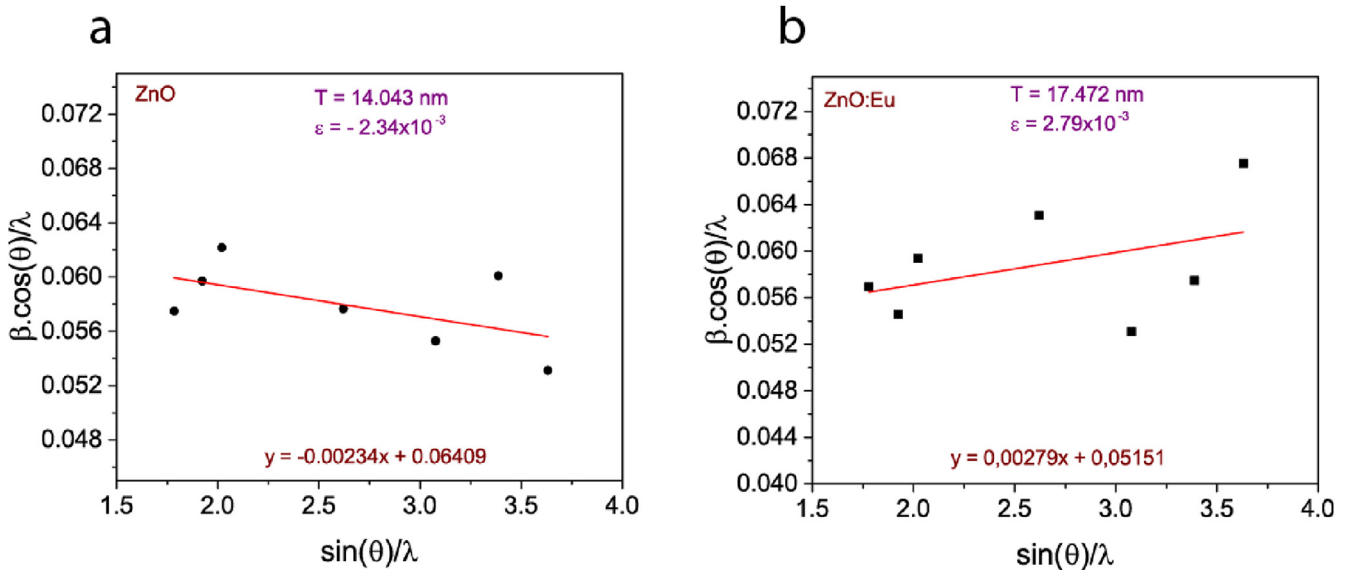


Fig. 4. Williamson-Hall plots of (a) undoped and (b) Eu-doped ZnO nanorods.

where  $R$  is the diffuse reflectance. Fig. 5 shows the K-M plots for Eu-doped and undoped ZnO nanorods, evidencing that the Eu incorporation causes a slight decrease in the optical band gap.

Theoretical modeling was performed at DFT in order to better understand these effects on its physical and chemical behavior, as well as, reveal changes in the electronic structure properties of such thin films. The success for describing physical and chemical properties in the solid state, in general, depended on accurate approximation on the band gap energy in the electronic structure calculations, i.e., since it is well known that the band gap energy provides remarkable information that can bring new scientific perspectives on the potential applications of these materials. We first investigated the band structures of both pure and Eu-doped ZnO models that are characterized by well-defined direct electronic transitions located at  $\Gamma$  point, as shown in Fig. 6(a,c). In particular, the band gap is 3.21 eV for the ZnO and 2.91 eV for the

Eu-doped ZnO, respectively, as a consequence of structural changes. In order to better understand this change in the electronic structure, we showed in Fig. 6(b,d) a detailed analysis of the DOS for both pure and Eu-doped ZnO models. Fig. 6(b) shows that the valence band (VB) consists mainly of O- $2p_x, p_y$  orbital levels, with minor contributions of the Zn- $3p$  and Zn- $3d_{(x-y)}^2$  orbital levels. On the other hand, the CB is composed mainly of the hybrid states of Zn- $3p$  and Zn- $4s$ , with minimum contributions from the O- $2p$  orbital levels. Due to the presence of 3d states in the VB, there is a strong bonding character between O and Zn, which is in good agreement with previous work [54]. In comparison to that, the projected DOS for Eu-doped ZnO model, as shown in Fig. 6(d), reveals that significant changes in both VB and CB. According to these results, the VB of Eu-doped ZnO consists mainly of the contribution of Zn 3d orbital levels, being the major contributor the  $3d_z^2$  orbital, while the O contribution is kept. Due to doping with Eu atoms, the band gap is significantly reduced and it can be clearly seen from Fig. 6(c and d) that the Eu atoms contribute strongly in the VB with the  $p_x$  and  $p_y$  orbital levels. Even with the reduction in the band gap energy the emission in the electromagnetic spectrum is kept in UVA region, ~386.24 nm and ~426.06, before and after doping with Eu, respectively, improving the efficiency in solar energy absorption that can at first be achieved for instance in its photovoltaic applications.

Topological analysis of the electron density can at first provide important information on its structures, in special regarding to chemical bonds, fundamental to understand the type of interaction between two atoms and the modification induced by structure rearrangements [42]. In Fig. 7(a and b) is presented the electron density  $\rho(r)$  and the Laplacian of the electron density ( $\nabla^2\rho(r)$ ), the blue (dashed) and red (solid) lines represent the depletion and concentration of the charge (negative and positive contours), respectively. As it is seen in Fig. 7(a), the electron density is more concentrated around the Eu nucleus, while for Zn atoms the density is more scattered. We then studied the Laplacian maps, which show an intense depletion around the Eu nucleus and a great proximity of the electronic density (bond critical point), which indicate that Eu-O bonds are more ionic than the Zn-O bonds (see Fig. 7(b)). Zn-O bond is classified as transitory bond, neither ionic nor covalent, although the bond critical point is almost equidistant from the two nuclear attractors, and there is a clear difference between the

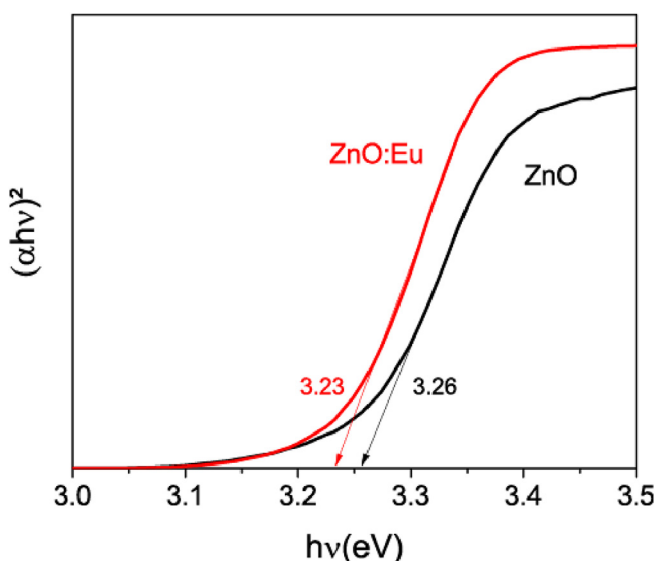
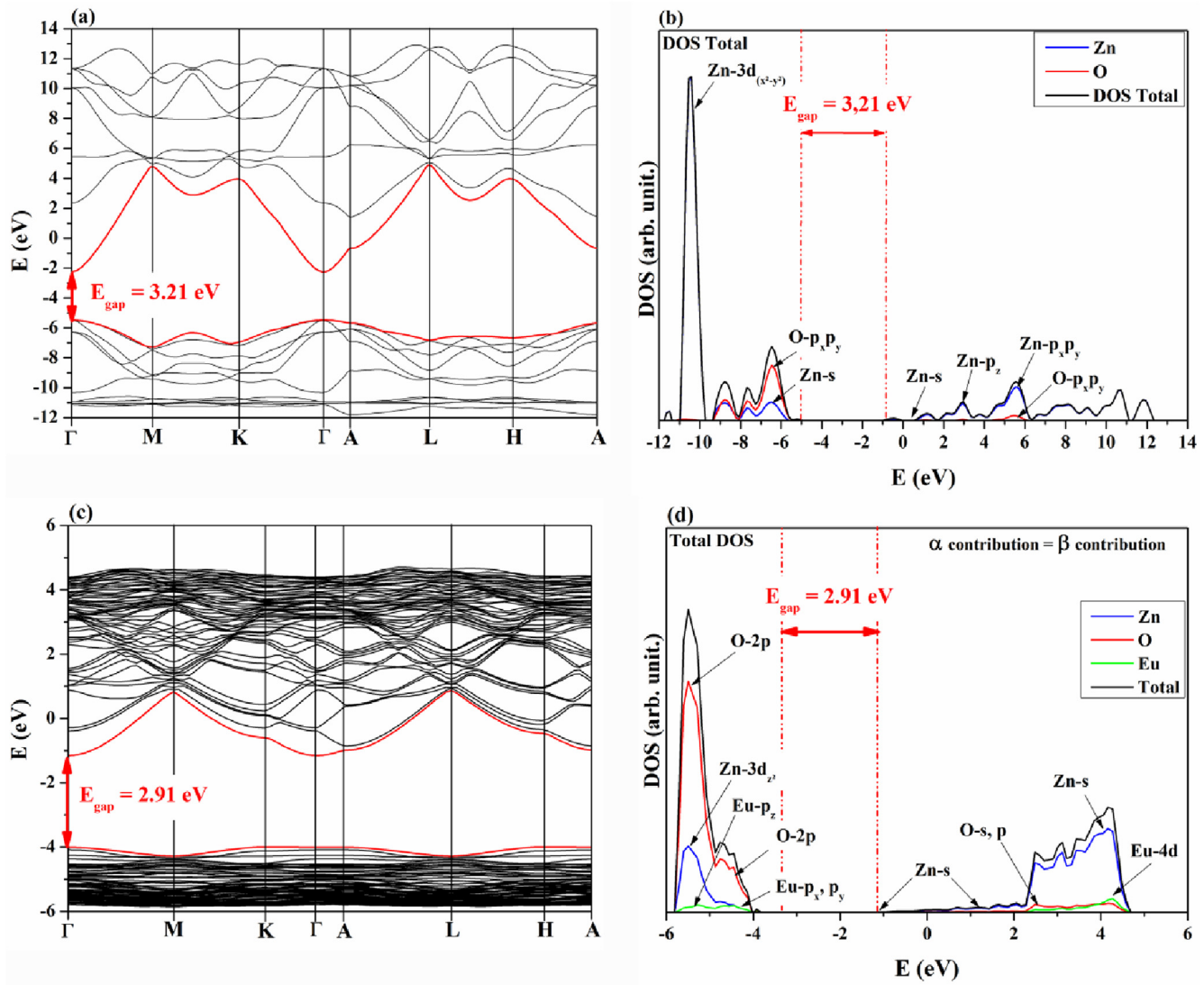
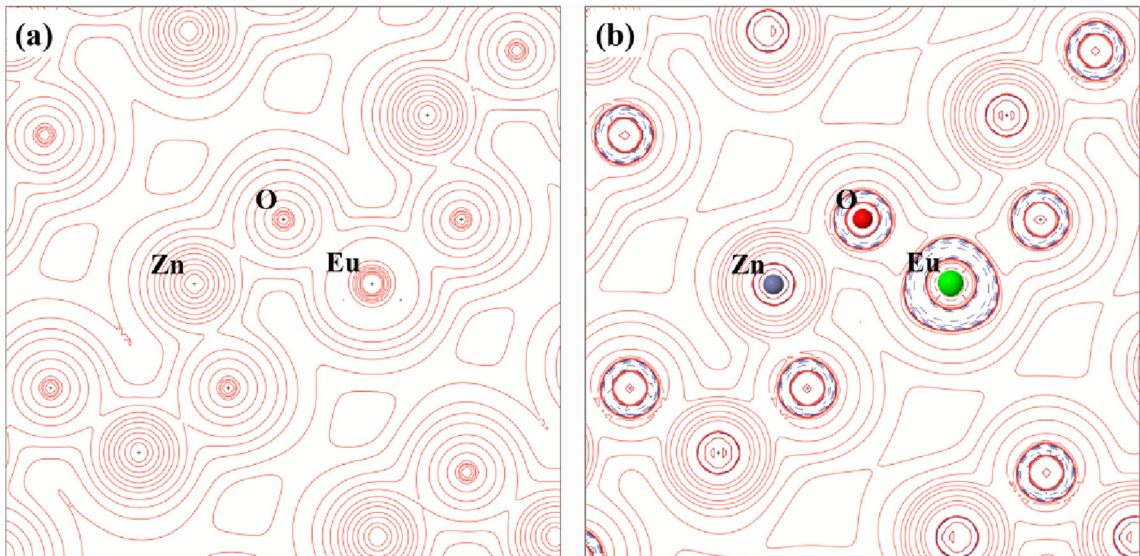


Fig. 5. Kubelka-Munk diffuse reflectance spectra for Eu-doped and undoped ZnO bandgap determination.



**Fig. 6.** (a,c) Band structures and (b,d) projected DOS of both pure (top) and Eu-doped ZnO (below), respectively.



**Fig. 7.** (a) electron density  $\rho(r)$  and (b) Laplacian of the electron density ( $\nabla^2\rho(r)$ ) of Eu-doped ZnO.

density of these two atoms, since it confirms confirm the most intense ionic character of this bond.

XPS analysis was used to investigate the surface chemical composition of the Eu-doped ZnO nanorods. The binding energies scale was calibrated with the C1s peak of carbon (284.6 eV). In all our measurements, low intensity carbon peaks (C-1s) were detected due to the exposure of the samples to air. Fig. 8(a) shows XPS spectra of the Zn-2p core level region with two intense peaks at 1021.4 and 1044.5 eV. These peaks are assigned to  $2p_{3/2}$  and  $2p_{1/2}$ , respectively, and the energetic separation of 23.1 eV are in good agreement with the related standard value (22.97 eV) [55]. While the spectra of the O-1s core level region is shown particularly in Fig. 8(b). In particular, the asymmetry of this peak was deconvoluted in two peaks at about 529.7 and 531.3 eV, which is assigned to stoichiometric (Zn-O) and defective ZnO (Zn-OH), respectively [56]. Based on the integrated areas of these peaks, the relative content was 64.4% of Zn-O and 35.5% of Zn-OH, respectively.

Fig. 9 shows the XPS spectra of Eu-3d core levels with the presence of peaks at 1125.3 and 1133.9 eV. These peaks are described as  $3d_{5/2}$  levels of  $\text{Eu}^{2+}$  and  $\text{Eu}^{3+}$ , respectively, which implies in the co-existence of both the oxidation states in the ZnO crystalline lattice [32]. The relative content was obtained by integration as ~29.1% of  $\text{Eu}^{2+}$  to ~70.9% of  $\text{Eu}^{3+}$ . Comparing these results, probably the  $\text{Eu}^{2+}$  is incorporated in the ZnO by the substitution of  $\text{Zn}^{2+}$  ions in the lattice while the trivalent species are on the surface of the nanorods, occupying the vacancies or in the grain boundaries [57]. The content of Europium on the surface region was calculated by the ratio between the integrated areas from the Europium and Zinc peaks and the obtained result was around of 10.51%.

Fig. 10(a) shows the photocurrent densities responses upon on/off lighting cycles with AM 1.5 radiation. Both the samples presented good stability during the measurement being evident the increase on the generated photocurrent ( $J_{\text{sc}}$ ) with the Eu-doping from 1.21 to 1.72 mA/cm<sup>2</sup>. The J-V curves of the cells based on Eu-doped and undoped ZnO nanorods were presented on Fig. 10(b), and their photovoltaic parameters are presented in Table 1. The open circuit voltage ( $V_{\text{oc}}$ ) and filling factor (ff) do not present significant changes with the doping process. However, the conversion efficiency values ( $\eta$ ) for the Eu-doped and undoped based DSSCs

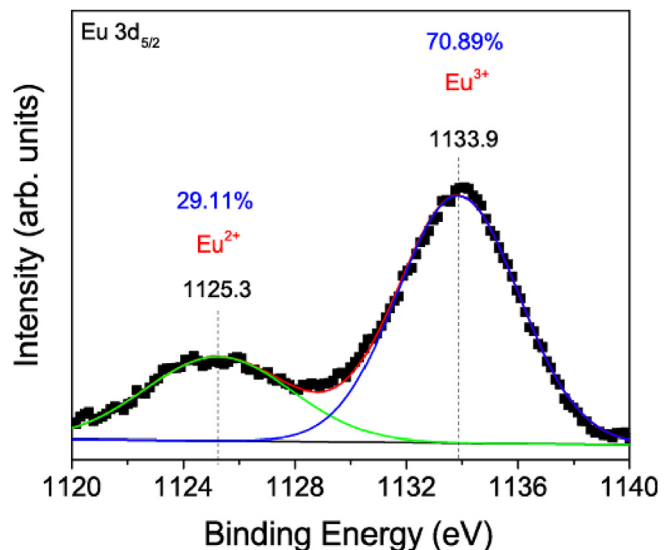


Fig. 9. XPS spectra of the Eu-3d<sub>5/2</sub> core level region of the nanorods.

were 0.50 and 0.34%, respectively, which implies in an increase around 45%. These values are in good agreement with the literature that shows a conversion efficiency around 0.38% for DSSCs in same conditions and based on undoped ZnO nanorods [58,59].

Mott-Schottky (MS) measurements were commonly used to estimate the flat band potential ( $V_{\text{fb}}$ ) of ZnO nanorods [60,61]. Fig. 10(c) shows the MS plots for Eu-doped and undoped nanorods arrays. In both samples, the positive slope in the linear region of the MS plots is due to fact that ZnO is a n-type semiconductor. The Eu-doped ZnO nanorods showed a positive shift in the  $V_{\text{fb}}$  values (from -0.36 V to -0.31 V). These findings are consistent with our theoretical calculations. Hence, this shift justifies the improvement of the DSSCs, since it causes an increase in the energy difference between the lowest unoccupied molecular orbital (LUMO) from the dye and the conduction band of the ZnO nanorods, which can improve the electronic injection efficiency of the N719 dye into the ZnO nanorod [32,62].

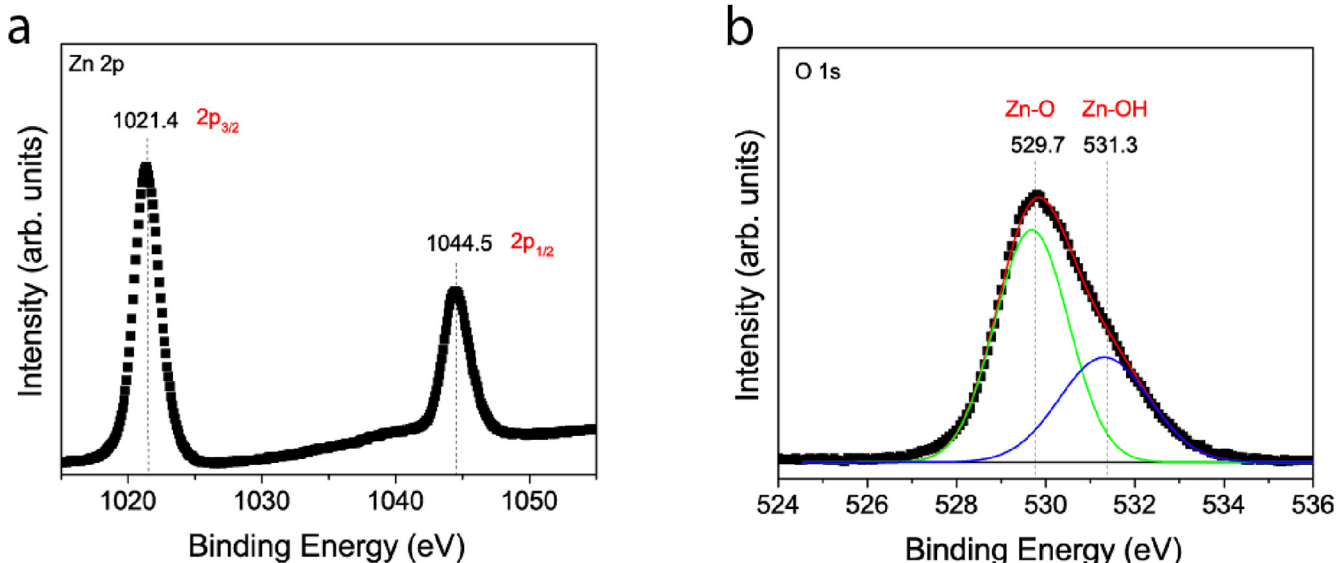
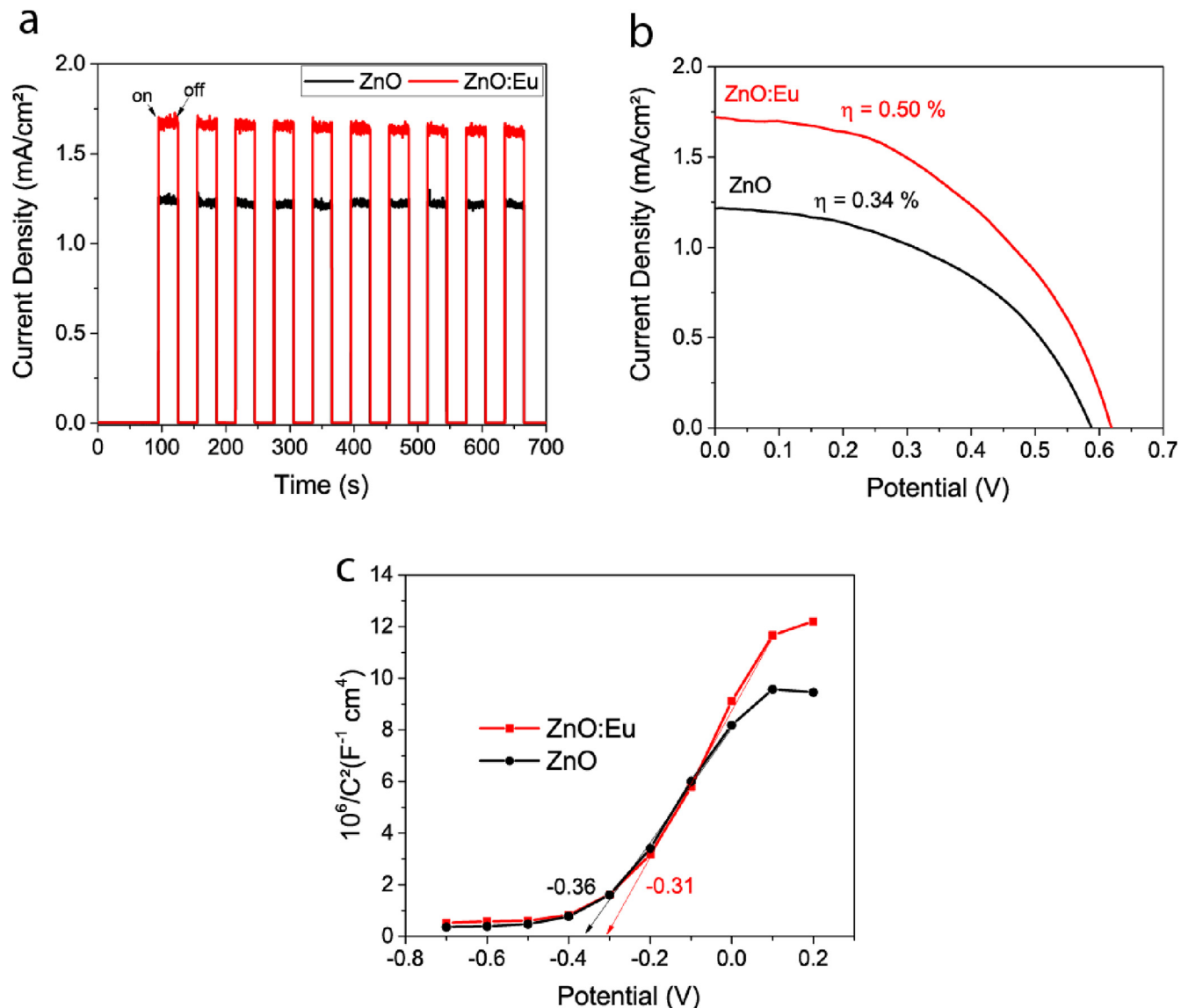


Fig. 8. (a) XPS spectra corresponding to the Zn-2p and (b) O-1s core level regions of the nanorods.



**Fig. 10.** (a) Photocurrent densities upon on/off light cycles, (b) J-V curves of DSCs fabricated with Eu-doped and undoped ZnO nanorods arrays, and (c) Mott-Schottky (MS) plots of Eu-doped and undoped ZnO nanorods.

**Table 1**  
Photovoltaic performance parameters of DSSCs.

Photoanode	J <sub>sc</sub> (mA cm <sup>-2</sup> )	V <sub>oc</sub> (V)	ff	η (%)
ZnO	1.21	0.59	0.48	0.34
ZnO:Eu	1.72	0.62	0.47	0.50

#### 4. Conclusion

Eu-doped ZnO nanorods was successfully synthesized and applied as photoanodes in dye sensitized solar cells. The doping of the ZnO nanorods with Eu was evidenced by XRD which evidencing a small shift on 2θ values of (100) diffraction peak for the Eu-doped nanorods, and also by XPS analysis, in which the content of Europium was around of 10.51% with relative content of ~29.1% of Eu<sup>2+</sup> and ~70.9% of Eu<sup>3+</sup>.

Our theoretical findings reveal the effect of Eu-doping on the electronic structure of ZnO and are in very good agreement with our experimental results. The improvement is assigned to the

better electronic injection efficiency from the dye to the CB of ZnO nanorods, i.e., due to the shift in the CB after the europium incorporation in the ZnO crystalline lattice.

The conversion efficiency values ( $\eta$ ) for the Eu-doped based DSSCs were 0.50%, which was around 45% higher in comparison with the undoped nanorods, (0.34%) showing the great potential from the practical point of view to increase the use of ZnO in solar cells.

#### Acknowledgments

The authors gratefully acknowledge financial support from CAPES, FAPEMIG, CNPq, Rede Mineira de Química.

#### References

- [1] J. Gong, K. Sumathy, Q. Qiao, Z. Zhou, Review on dye-sensitized solar cells (DSSCs): advanced techniques and research trends, *Renew. Sustain. Energy Rev.* 68 (2017) 234–246.
- [2] A. Mohammad Bagher, Types of solar cells and application, *Am. J. Opt. Photon.* 3 (2015) 94.
- [3] A. Polman, M. Knight, E.C. Garnett, B. Ehrler, W.C. Sinke, Photovoltaic materials

- present efficiencies and future challenges, *Science* 352 (2016) 307.
- [4] C. Hanhong, P. Aurelien Du, S. Gaurav, Z. Jian, L. Yicheng, Dye-sensitized solar cells using ZnO nanotips and Ga-doped ZnO films, *Semicond. Sci. Technol.* 23 (2008), 045004.
- [5] B. O'Regan, M. Gratzel, A low-cost, high-efficiency solar cell based on dye-sensitized colloidal TiO<sub>2</sub> films, *Nature* 353 (1991) 737–740.
- [6] V. Sugathan, E. John, K. Sudhakar, Recent improvements in dye sensitized solar cells: a review, *Renew. Sustain. Energy Rev.* 52 (2015) 54–64.
- [7] S. Sharma, B. Siwach, S.K. Ghoshal, D. Mohan, Dye sensitized solar cells: from genesis to recent drifts, *Renew. Sustain. Energy Rev.* 70 (2017) 529–537.
- [8] D.-y. Son, J.-h. Im, H.-s. Kim, N.-g. Park, 11% efficient perovskite solar cell based on ZnO nanorods: an effective charge collection system, *J. Phys. Chem. C* 118 (2014), 140317091621004.
- [9] A. Omar, H. Abdullah, Electron transport analysis in zinc oxide-based dye-sensitized solar cells: a review, *Renew. Sustain. Energy Rev.* 31 (2014) 149–157.
- [10] M. Rani, S.K. Tripathi, A comparative study of nanostructured TiO<sub>2</sub>, ZnO and bilayer TiO<sub>2</sub>/ZnO dye-sensitized solar cells, *J. Electron. Mater.* 44 (2015) 1151–1159.
- [11] R. Vittal, K.-C. Ho, Zinc oxide based dye-sensitized solar cells: a review, *Renew. Sustain. Energy Rev.* (2016) 1–15.
- [12] A. Kolodziejczak-Radzimska, T. Jesionowski, Zinc oxide—from synthesis to application: a review, *Materials* 7 (2014) 2833–2881.
- [13] M.D. Tyona, R.U. Osuji, F.I. Ezema, A review of zinc oxide photoanode films for dye-sensitized solar cells based on zinc oxide nanostructures, *Adv. Nano Res.* 1 (2013) 43–58.
- [14] M. Gong, X. Xu, Z. Yang, Y. Liu, H. Lv, L. Liu, Structure, photoluminescence and wettability properties of well arrayed ZnO nanowires grown by hydrothermal method, *J. Nanosci. Nanotechnol.* 10 (2010) 7762–7765.
- [15] P.R. Deshmukh, Y. Sohn, W.G. Shin, Chemical synthesis of ZnO nanorods: investigations of electrochemical performance and photo-electrochemical water splitting applications, *J. Alloys Compd.* 711 (2017) 573–580.
- [16] M. Kaur, S. Kailasaganapathi, N. Ramgir, N. Datta, S. Kumar, A.K. Debnath, D.K. Aswal, S.K. Gupta, Gas dependent sensing mechanism in ZnO nanobel sensor, *Appl. Surf. Sci.* 394 (2017) 258–266.
- [17] X.Y. Kong, Z.L. Wang, Spontaneous polarization-induced nanohelixes, nanosprings, and nanorings of piezoelectric nanobelts, *Nano Lett.* 3 (2003) 1625–1631.
- [18] Y. Peng, L. Bao, Controlled-synthesis of ZnO nanorings, *Front. Chem. China* 3 (2008) 458–463.
- [19] Y. Wang, X. Chen, J. Zhang, Z. Sun, Y. Li, K. Zhang, B. Yang, Fabrication of surface-patterned and free-standing ZnO nanobowls, *Colloids Surf. A Physicochem. Eng. Asp.* 329 (2008) 184–189.
- [20] P. Uthirakumar, S. Muthulingam, B.D. Ryu, J.H. Kang, A. Periyasamy, M. Prabakaran, C.H. Hong, Organic solvent assisted growth of flower-like ZnO for enhanced photocatalytic activities, *Curr. Nanosci.* 9 (2013) 335–340.
- [21] X. Wu, W. Cai, F.-Y. Qu, Spontaneous formation of single crystal ZnO nanohelices, *Chin. Phys. B* 18 (2009) 1669.
- [22] M. Quintana, T. Edvinsson, A. Hagfeldt, G. Boschloo, Comparison of dye-sensitized ZnO and TiO<sub>2</sub> solar cells: studies of charge transport and carrier lifetime, *J. Phys. Chem. C* 111 (2007) 1035–1041.
- [23] J.B. Baxter, E.S. Aydil, Nanowire-based dye-sensitized solar cells, *Appl. Phys. Lett.* 86 (2005), 053114.
- [24] M. Law, L.E. Greene, J.C. Johnson, R. Saykally, P. Yang, Nanowire dye-sensitized solar cells, *Nat. Mater.* 4 (2005) 455–459.
- [25] L. Lu, R. Li, T. Peng, K. Fan, K. Dai, Effects of rare earth ion modifications on the photoelectrochemical properties of ZnO-based dye-sensitized solar cells, *Renew. Energy* 36 (2011) 3386–3393.
- [26] M. Ye, X. Wen, M. Wang, J. Iocozzia, N. Zhang, C. Lin, Z. Lin, Recent advances in dye-sensitized solar cells: from photoanodes, sensitizers and electrolytes to counter electrodes, *Mater. Today* 18 (2015) 155–162.
- [27] S. Yun, J. Lee, J. Chung, S. Lim, Improvement of ZnO nanorod-based dye-sensitized solar cell efficiency by Al-doping, *J. Phys. Chem. Solids* 71 (2010) 1724–1731.
- [28] V. Kumar, N. Singh, V. Kumar, L.P. Purohit, A. Kapoor, O.M. Ntwaeborwa, H.C. Swart, Doped zinc oxide window layers for dye sensitized solar cells, *J. Appl. Phys.* 114 (2013), 134506.
- [29] M. Samadi, M. Zirak, A. Naseri, E. Khorashadizade, A.Z. Moshfegh, Recent progress on doped ZnO nanostructures for visible-light photocatalysis, *Thin Solid Films* 605 (2016) 2–19.
- [30] Z.-L. Huang, C.-M. Chen, Z.-K. Lin, S.-H. Yang, Efficiency enhancement of regular-type perovskite solar cells based on Al-doped ZnO nanorods as electron transporting layers, *Superlattices Microstruct.* 102 (2017) 94–102.
- [31] R. Swapna, T. Srinivasareddy, K. Venkateswarlu, M.C.S. Kumar, Effect of post-annealing on the properties of Eu doped ZnO nano thin films, *Procedia Mater. Sci.* 10 (2015) 723–729.
- [32] J.X. Zhao, X.H. Lu, Y.Z. Zheng, S.Q. Bi, X. Tao, J.F. Chen, W. Zhou, Eu doping for hierarchical ZnO nanocrystalline aggregates based dye-sensitized solar cell, *Electrochim. Commun.* 32 (2013) 14–17.
- [33] R. Dovesi, R. Orlando, A. Erba, C.M. Zicovich-Wilson, B. Civalleri, S. Casassa, L. Maschio, M. Ferrabone, M. De La Pierre, P. D'Arco, Y. Noël, M. Causà, M. Rérat, B. Kirtman, CRYSTAL14: a program for the ab initio investigation of crystalline solids, *Int. J. Quant. Chem.* 114 (2014) 1287–1317.
- [34] J.E. Jaffe, A.C. Hess, Hartree-Fock study of phase changes in ZnO at high pressure, *Phys. Rev. B Condens. Matter* 48 (1993) 7903–7909.
- [35] T. Bredow, K. Jug, R.A. Evarestov, Electronic and magnetic structure of ScMnO<sub>3</sub>, *Phys. Status Solidi (b)* 243 (2006) R10–R12.
- [36] M.M. Ferrer, Y.V.B. de Santana, C.W. Raubach, F.A. La Porta, A.F. Gouveia, E. Longo, J.R. Sambrano, Europium doped zinc sulfide: a correlation between experimental and theoretical calculations, *J. Mol. Model.* 20 (2014) 2375.
- [37] L. Maron, O. Eisenstein, Do f electrons play a role in the Lanthanide–Ligand bonds? A DFT study of In(NR<sub>2</sub>)<sub>3</sub>; R = H, SiH<sub>3</sub>, *J. Phys. Chem. A* 104 (2000) 7140–7143.
- [38] M.M. Nolasco, P.D. Vaz, L.D. Carlos, The role of 4,7-disubstituted phenothiazine ligands in energy transfer of europium(III) complexes: a DFT study, *N. J. Chem.* 35 (2011) 2435–2441.
- [39] M. Dolg, H. Stoll, A. Savin, H. Preuss, Energy-adjusted pseudopotentials for the rare earth elements, *Theor. Chim. Acta* 75 (1989) 173–194.
- [40] M. Dolg, H. Stoll, H. Preuss, A combination of quasirelativistic pseudopotential and ligand field calculations for lanthanoid compounds, *Theor. Chim. Acta* 85 (1993) 441–450.
- [41] N.L. Marana, F.A. La Porta, E. Longo, J.R. Sambrano, Theoretical study on band alignment mechanism for the ZnO@ZnS interface of core-shell structures, *Curr. Phys. Chem.* 5 (2015) 327–336.
- [42] N.L. Marana, S. Casassa, E. Longo, J.R. Sambrano, Structural, electronic, vibrational, and topological analysis of single-walled zinc oxide nanotubes, *J. Phys. Chem. C* 120 (2016) 6814–6823.
- [43] N.L. Marana, V.M. Longo, E. Longo, J.B.L. Martins, J.R. Sambrano, Electronic and structural properties of the (1010) and (1120) ZnO surfaces, *J. Phys. Chem. A* 112 (2008) 8958–8963.
- [44] A. Nouri, A. Beniaiche, B.M. Soucase, H. Guessas, A. Azizi, Photoluminescence study of Eu+3 doped ZnO nanocolumns prepared by electrodeposition method, *Optik* 139 (2017) 104–110.
- [45] M. Skompska, K. Zarebska, Electrodeposition of ZnO nanorod arrays on transparent conducting substrates—a review, *Electrochim. Acta* 127 (2014) 467–488.
- [46] L. Vayssières, K. Keis, S.-E. Lindquist, A. Hagfeldt, Purpose-built anisotropic metal oxide material: 3D highly oriented microrod array of ZnO, *J. Phys. Chem. B* 105 (2001) 3350–3352.
- [47] A.J. Bard, L.R. Faulkner, *Electrochemical Methods: Fundamentals and Applications*, 2 ed., John Wiley & Sons Inc, 2000.
- [48] M. Gusatti, D.A.R. Souza, N.C. Kuhnhen, H.G. Riella, Growth of variable aspect ratio ZnO nanorods by solothermal processing, *J. Mater. Sci. Technol.* 31 (2015) 10–15.
- [49] N.S. Ridhuan, K. Abdul Razak, Z. Lockman, A. Abdul Aziz, Structural and morphology of ZnO nanorods synthesized using ZnO seeded growth hydrothermal method and its properties as UV sensing, *PLoS One* 7 (2012).
- [50] J. Yang, X. Li, J. Lang, L. Yang, M. Wei, M. Gao, X. Liu, H. Zhai, R. Wang, Y. Liu, J. Cao, Synthesis and optical properties of Eu-doped ZnO nanosheets by hydrothermal method, *Mater. Sci. Semicond. Process.* 14 (2011) 247–252.
- [51] F.A. La Porta, J. Andrés, M.S. Li, J.R. Sambrano, J.A. Varela, E. Longo, Zinc blende versus wurtzite ZnS nanoparticles: control of the phase and optical properties by tetrabutylammonium hydroxide, *Phys. Chem. Chem. Phys.* 16 (2014) 20127.
- [52] H. Yadav, N. Sinha, S. Goel, B. Kumar, Eu-doped ZnO nanoparticles for dielectric, ferroelectric and piezoelectric applications, *J. Alloys Compd.* 689 (2016) 333–341.
- [53] G.K. Williamson, W.H. Hall, X-ray line broadening from filed aluminium and wolfram, *Acta Metall.* 1 (1953) 22–31.
- [54] F.A. La Porta, J. Andres, M.V.G. Vismara, C.F.O. Graeff, J.R. Sambrano, M.S. Li, J.A. Varela, E. Longo, Correlation between structural and electronic order-disorder effects and optical properties in ZnO nanocrystals, *J. Mater. Chem. C* 2 (2014) 10164–10174.
- [55] J.F. Moulder, J. Chastain, *Handbook of X-ray Photoelectron Spectroscopy: a Reference Book of Standard Spectra for Identification and Interpretation of XPS Data*, Physical Electronics Division, Perkin-Elmer Corporation, 1992.
- [56] O. Lupon, T. Pauporté, B. Viana, P. Aschehoug, M. Ahmadi, B.R. Cuenna, Y. Rudzhevich, Y. Lin, L. Chow, Eu-doped ZnO nanowire arrays grown by electrodeposition, *Appl. Surf. Sci.* 282 (2013) 782–788.
- [57] S.M. Ahmed, P. Szymanski, M.A. El-Sayed, Y. Badr, L.M. El-Nadi, The photoluminescence properties of undoped & Eu-doped ZnO thin films grown by RF sputtering on sapphire and silicon substrates, *Appl. Surf. Sci.* 359 (2015) 356–363.
- [58] R. Kumar, A. Umar, G. Kumar, H.S. Nalwa, A. Kumar, M.S. Akhtar, Zinc oxide nanostructure-based dye-sensitized solar cells, *J. Mater. Sci.* 52 (2017) 4743–4795.
- [59] K. Nadarajah, A.F. Khan, N.A. Rahim, Chemically grown ZnO nanorods for dye-sensitized solar cells, in: 3rd IET International Conference on Clean Energy and Technology (CEAT) 2014, 2014, pp. 1–5.
- [60] T. Majumder, J.J.L. Hmar, K. Debnath, N. Gogurla, J.N. Roy, S.K. Ray, S.P. Mondal, Photoelectrochemical and photosensing behaviors of hydrothermally grown ZnO nanorods, *J. Appl. Phys.* 116 (2014), 034311.
- [61] I. Mora-Seró, F. Fabregat-Santiago, B. Denier, J. Bisquert, R. Tena-Zaera, J. Elias, C. Lévy-Clément, Determination of carrier density of ZnO nanowires by electrochemical techniques, *Appl. Phys. Lett.* 89 (2006) 28–30.
- [62] M. Gratzel, J.R. Durrant, *Dye-Sensitised Mesoscopic Solar Cells, Nanostructured and Photoelectrochemical Systems for Solar Photon Conversion*, 2008, pp. 503–536.